CONTRAST MEDIA & MOLECULAR IMAGING

Received: 23 July 2013, Revised: 20 September 2013, Accepted: 29 September 2013, Published online in Wiley Online Library

(wileyonlinelibrary.com) DOI: 10.1002/cmmi.1576

Bifunctional Gd(III) and Tb(III) chelates based on a pyridine–*bis*(iminodiacetate) platform, suitable optical probes and contrast agents for magnetic resonance imaging

Sophie Laurent[a]*, Luce Vander Elst[a], Chantal Galaup[b,c], Nadine Leygue[b,c], Sébastien Boutry[a,d], Claude Picard[b,c] and Robert. N. Muller[a,d]

To study the physicochemical properties of lanthanide complexes derived from a bifunctional chelating agent based on a PMN-tetraacetic acid moiety {PMN-tetraacetic acid (1): [2,6-pyridinediyl*bis*(methylene nitrilo)-tetraacetic acid]}, 4-carboxylic acid substituted pyridine derivative (2) was synthesized. This ligand forms heptadentate (N_3O_4) Ln(III) complexes (Ln = Gd, Eu, Tb), with two water molecules completing the inner coordination sphere of the metal. The parameters that govern the relaxivity of the Gd(III) complex and the luminescence of Eu(III) and Tb(III) complexes were obtained by ^{17}O and ^{1}H NMR studies and time-resolved fluorescence experiments, respectively. The gadolinium and terbium complexes show interesting properties either for MRI or FOR optical imaging; that is, for the Gd complex, a high proton relaxivity ($r_1 = 6.4\ s^{-1}\ mM^{-1}$ at 20 MHz) with short water residence time ($\tau_M = 38.5$ ns); for the Tb complex, a luminescence lifetime of 1.22 ms at room temperature and a luminescence quantum yield of 10%. The kinetic stability of these complexes toward blood protein, cation or bioactive oxyanion was also examined. The Gd(2)$(H_2O)_2$ complex does not interact with human serum albumin, but undergoes a transmetalation reaction with Zn(II) in a phosphate buffer solution (pH 7.4), rather similar to that of Gd–DTPA–BMA(H_2O). On the other hand, as observed for Eu and Tb complexes, these chelates do not form ternary complexes with bidentate anions such as L-lactate, citrate or carbonate. Finally, a phosphatidylserine-specific hexapeptide (TLVSSL) was grafted on Gd or Tb chelates, and the Gd–peptide conjugate was used *in vitro* for targeting apoptotic cells. Copyright © 2014 John Wiley & Sons, Ltd.

Keywords: pyridine-*bis*(iminodiacetate) chelators; Ln(III) chelates; magnetic resonace imaging (MRI); luminescence spectroscopy; apoptotic cells; molecular imaging

1. INTRODUCTION

Imaging probes based on lanthanide trivalent ions, Ln(III), are of special interest because of the unique magnetic and photophysical properties of these ions. The high magnetic moment (7.9 BM) coupled with a long electronic relaxation time (10^{-8}– 10^{-9} s) of Gd(III) makes this ion available as an efficient paramagnetic center for increasing and controlling the magnetic relaxation of water protons (1). The inner-shell nature of 4f electrons results in Ln(III) ions having remarkable luminescence characteristics, such as easily recognizable line-like emission bands in the visible (400–700 nm) and near-infrared (800–2000 nm) regions, as well as long-lived excited states (μs and ms domains), which make them attractive as alternative optical bioprobes to conventional organic dyes (2). As a consequence, Gd(III) complexes are currently used to enhance the intrinsic contrast of magnetic resonance images in clinical studies (~30–40% MRI exams), and Eu(III), Tb(III) or Yb(III), Nd(III) complexes are gaining importance in *in vitro* optical imaging (time-resolved luminescence microscopy, TRLM) (3,4).

Numerous research groups have developed different structures of small molecular Ln(III) chelates for their magnetic or optical properties (5,6). However, so far, only a few efficient lanthanide chelators for this dual modality approach have been developed. An example is provided by the use of a cyclen-based chelate containing two phosphonic acid groups for metal chelation, a heterocyclic chromophore for europium sensitization and a ligand for a peripherical benzodiazepine receptor (7). A cocktail of these two monoaqua complexes of Eu(III) and Gd(III) derived from this chelate was used successfully for imaging of PBR-overexpressing

* *Correspondence to: S. Laurent, NMR and Molecular Imaging Laboratory, Department of General, Organic and Biomedical Chemistry, Université de Mons, B-7000 Mons, Belgium. E-mail: sophie.laurent@umons.ac.be*

a *S. Laurent, L. Vander Elst, S. Boutry, R. N. Muller*
NMR and Molecular Imaging Laboratory, Department of General, Organic and Biomedical Chemistry, Université de Mons, B-7000, Mons, Belgium

b *C. Galaup, N. Leygue, C. Picard*
Université de Toulouse; UPS; Laboratoire de Synthèse et Physico-Chimie de Molécules d'Intérêt Biologique, SPCMIB, 118 route de Narbonne, F-31062, Toulouse cedex 9, France

c *C. Galaup, N. Leygue, C. Picard*
CNRS; Laboratoire de Synthèse et Physico-Chimie de Molécules d'Intérêt Biologique, SPCMIB, UMR-5068, 118 Route de Narbonne, F-31062, Toulouse cedex 9, France

d *S. Boutry, R. N. Muller*
Center for Microscopy and Molecular Imaging (CMMI), Académie Wallonie-Bruxelles, B 6041, Gosselies, Belgium

C6 glioblastoma cells. More recently, we reported a heptadentate acyclic ligand (PMN-tetraacetic acid, compound **1**, Scheme 1) based on a pyridine core as a chromophoric group and two iminodiacetate arms as Ln(III) chelating moiety and which yields diaqua Eu(III) and Gd(III) complexes with good luminescent and MR properties, respectively (8). In the Gd(III) complex, the presence of two metal-bound water molecules ensures an MRI efficacy with a larger proton relaxivity than that found in mono-aqua Gd(III)-based contrast agents used in clinical practice. For Eu(III) chelates, this hydration sphere does not impair the luminescence efficiency which remains competitive with that of some Eu(III)-based commercial luminescent probes. Moreover, these complexes are characterized by an attractive stability in aqueous solutions at physiological pH (log K_{cond} Gd = 16.4, log K_{cond} Eu = 16.6, pH 7.3) (9). These values are in the range of those of Gd(III) chelates used in clinical practice; a similar conditional stability constant [log K_{cond} = 14.9 pH 7.4 (10)] has been established for Gd–DTPA–BMA (Omniscan®). PMN-tetraacetic acid and derivatives were also recently proposed as near infrared luminescent reporters when complexed to Nd(III) or Yb(III), but with significantly lower quantum yields than those observed for the corresponding Eu(III) and Tb(III) complexes (11). PMN tetraacetic acid derivatives were also recently used as Eu(III) optical or Gd(III) resonance magnetic probes for a few biological applications (12–14). It therefore appeared that the PMN-tetraacetic acid scaffold may be of interest in finding dual imaging agents.

However, PMN tetraacetic acid is a basic structure that does not allow biomolecules derivatization, whereas in several applications, covalent conjugation of the chelate to bioactive molecules is required. In this direction, we decided to use a PMN tetraacetic acid chelator substituted by a carbomethoxy/carboxylic acid group on 4-position of the pyridine ring as a bifunctional chelating agent (**2**, Scheme 1). This aromatic functionality is amenable to covalent biological coupling, directly or through the use of heterobifunctional cross-linking reagents (15). Moreover, this strategy avoids the unsymmetrical functionalization of the chelating iminodiacetate moiety involving tedious synthetic protocols and low yields (16,17). In this work, we report a comprehensive study of magnetic and photophysical properties of the corresponding Gd(III) and Eu (III), Tb(III) chelates, respectively (compounds **6–8**, Scheme 1), with the objective of evaluating the parameters that determine proton relaxivity or luminescence. We demonstrate that the bifunctional Gd(III) and Tb(III) chelates are amenable to direct covalent peptide coupling. In addition, the Gd(III) chelate grafted with a phosphatidylserine -specific hexapeptide (TLVSSL) was evaluated *in vitro* for the targeting of apoptotic cells.

2. RESULTS AND DISCUSSION

2.1. Ligand and complexes synthesis

Ligand **1** was prepared as described in the literature (18) and the synthesis of ligand **2** is depicted in Scheme 2. It was obtained by the nucleophilic substitution of 2,6-*bis*(bromomethyl)pyridine-4-carboxylic acid methyl ester **14** with di-*tert*-butyl iminodiacetate to form the fully protected compound **16**. Subsequent hydrolysis under acid conditions (HCl 6 M) of the four aliphatic and the aromatic carboxylic ester functions of **16** afforded the target pentaacid derivative **2** as its trichlorhydrate salt.

The key trifunctionalized pyridine **14** was first obtained in four steps from commercial 2,6-lutidine-1-oxide following literature procedures (19–21). *O*-Methylation of this compound with dimethyl sulfate followed by treatment with aqueous potassium cyanide gave 4-cyano-2,6-lutidine **12** in moderate yield [29 vs 40% reported (21)]. Successive hydrolysis of the cyano function under basic conditions and esterification of the resulting carboxylic group with MeOH/H^+ afforded **13** in a satisfactory yield after chromatographic purification on silica gel (78% yield for these two steps). Attempts to obtain *bis*-bromo derivative **14** by a classical and direct free-radical bromination with stoichiometric amounts of NBS (*N*-bromo succinimide) in CCl_4 or C_6H_6 resulted in low yield (< 15%) after a critical purification process owing to the presence of polybrominated compounds. However, overbromination of benzylic groups of **13** with a large excess of NBS in CCl_4 and then chemoselective reduction back with diethyl phosphite–Hunig's base system (22) at room temperature afforded the desired *bis*-bromo compound in 57% yield. Compound **14** was also prepared in a higher overall yield (41 vs 13%) and using a two-step procedure from commercial methylisonicotinate. As a matter of fact, during the course of this work, Lebeau *et al*. reported a straightforward synthesis of *bis*-2,6-hydroxymethyl pyridine compound **15** by double addition of nucleophilic hydroxymethyl radicals onto protonated nicotinate (14). However, no detailed experimental part or characterization of the product was reported. In our hands, this Minisci reaction afforded compound **15** in a satisfactory 68% yield after column chromatography. Diol **15** was then brominated with phosphorus tribromide by standard methodology in 61% yield.

The Ln(III) chelates derived from ligands **1** and **2** were prepared in water solutions with a slight molar excess (ca 10%) of the lanthanide salt ($LnCl_3 6H_2O$) to avoid any presence of free ligand. After purification, the isolated samples (80–90% yield) gave a negative reaction with the Arsenazo test and no peak ascribable to the free ligand was obtained in their ESI mass spectrum.

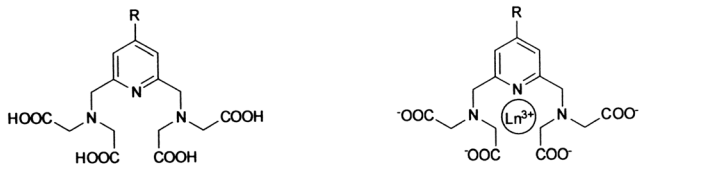

Scheme 1. Chemical structure of the ligands and lanthanide(III) complexes.

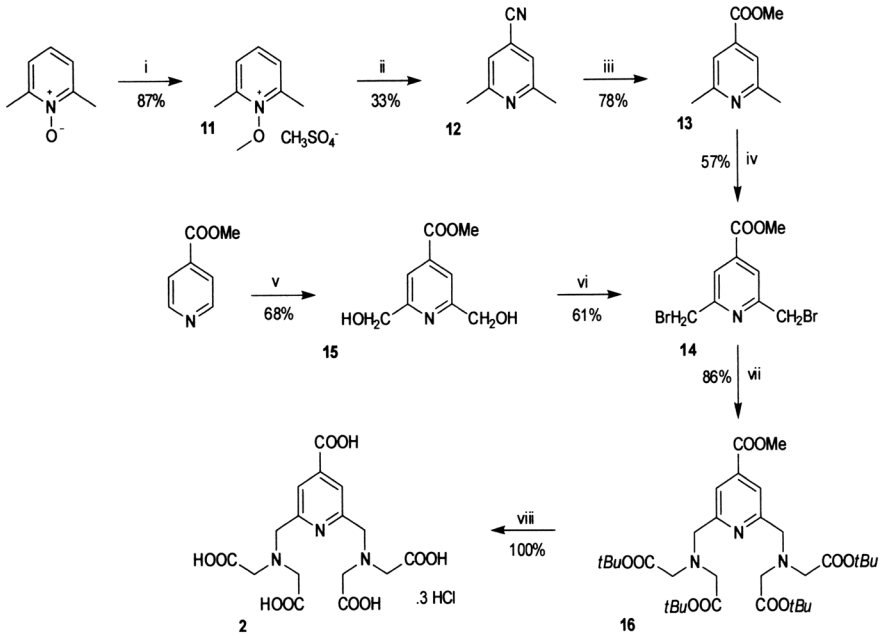

Scheme 2. Synthesis of ligand **2**. *Reagents and conditions*: (i) $(Me)_2SO_4$, 80 °C, 3 h; (ii) KCN, H_2O, 25 °C, 4 days; (iii) NaOH 2.5 N, EtOH, 100 °C, 5 h then conc. H_2SO_4 cat., MeOH, reflux, 24 h; (iv) NBS, benzoylperoxide cat., hυ , CCl_4, reflux, 7.5 h then $HP(O)(OEt)_2$, iPr_2NEt, THF, 0–25 °C, 18 h; (v) $(NH_4)_2S_2O_8$, H_2SO_4 cat., MeOH, H_2O, reflux, 20 h; (vi) PBr_3, $CHCl_3$, reflux, 20 h; (vii) $HN(CH_2COOtBu)_2$, Na_2CO_3, CH_3CN, reflux, 16 h; (viii) HCl 6 N, reflux, 48 h.

To demonstrate the potential utility of Ln(III) chelates derived from ligand **2** as reagents for peptide labeling, the corresponding Gd(III) and Tb(III) chelates (6,8) were grafted at the *N*-terminus of a $NH_2(CH_2CH_2O)_2CH_2COTLVSSL$ peptide (Scheme 3). This linear 6-mer peptide was previously identified by *ex vivo* phage display technology as a phosphatidylserine-recognizing and specific moiety and may possibly serve as a targeting vector for development of molecular probes for imaging of apoptosis (23). Activation of the noncoordinated aromatic carboxylate function of the chelates **6** and **8** was achieved *in situ* with EDCI·HCl [EDCI = 1-ethyl-3-(3-dimethylaminopropyl) carbodiimide] in water (pH 7) containing NHS-3-sulfonic acid (NHS = *N*-hydroxysuccinimide). The subsequent conjugation reaction between this NHS ester and one equivalent of the hexapeptide attached to a 8-amino-3,6-dioxaoctanoyl linker was monitored by MS analyses and afforded the bioconjugates **9** and **10** in 56 and 54% yields, respectively, after purification by dialysis. The purity of these compounds was established on the basis of the RP-HPLC chromatograms and their structure determined by high-resolution mass spectrometry (HRMS) analyses.

2.2. Relaxometric studies

The efficiency of paramagnetic complexes as MRI contrast agents depends on several parameters related to the outer- and inner-sphere contributions to the water proton relaxation rates. The inner-sphere contribution described by Solomon (24) and Bloembergen (25) results from the presence of one (or more) water molecule(s) in the first coordination sphere of the ion and from its (their) exchange with bulk water. It is thus closely related to the distance between the proton of the coordinated water molecule and the ion (r), to the rotational mobility of the hydrated complex (τ_R) and thus to its size, and to the residence time of the water molecule (τ_M). The outersphere mechanism as described by Freed (26) comes from the magnetic interaction between unbound water molecules diffusing in the close proximity of the ion. This mechanism depends on the distance of closest approach between the water molecules and the ion (d) and on the relative translational diffusion constant (D). For some complexes, an additional second sphere contribution has been involved (27). This contribution results from a second sphere of hydration molecules exchanging with bulk water. It is described by a model similar to the inner-sphere one but the distance of interaction (r_{SS}) is larger and the exchange rate of the water molecules is much faster. Among these, the number of coordinated water molecules (q) and their residence time can be measured by oxygen-17 NMR. The rotational correlation time and the electronic relaxation properties are extracted from the analysis of the NMRD profiles.

The proton relaxivities of the three Gd complexes **3**, **6** and **9** as measured at 310 K and 20 MHz, are given in Tables 1 and 2. At

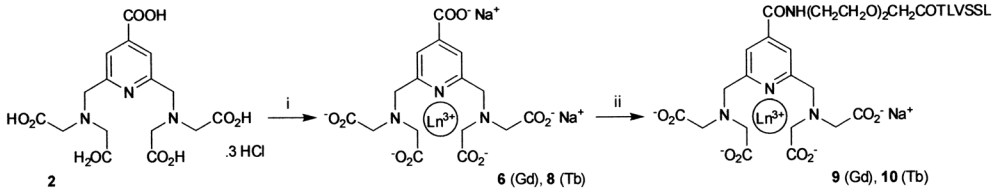

Scheme 3. Synthesis of peptide conjugates **9** and **10**. *Reagents and conditions*: (i) $LnCl_3.6H_2O$ (1.1 equiv.), H_2O, pH 7.4, room temperature, 24 h. (ii) EDCI. HCl, NHS, H_2O, room temperature, 24 h; then $NH_2(CH_2CH_2O)_2CH_2COTLVSSL$ (1 equiv.), room temperature, 48 h.

Table 1. Parameters obtained from the theoretical fittings of the O-17 data of Gd(III) complexes 3, 6 and 9 and comparison with the monoaqua complex (Gd–DTPA) and the diaqua complex (Gd–PCTA12)

Compounds	$\Delta H^{\#}$ (kJ/mol)	$\Delta S^{\#}$ (J mol^{-1} K^{-1})	$A/\hbar$ (10^6 rad s^{-1})	B (10^{20} s^{-2})	τ_V (ps)	E_V (kJ mol^{-1})
Gd 3	52.2 ± 0.07	66 ± 0.5	−4.17 ± 0.03	8.13 ± 0.2	14.8 ± 0.3	5.31 ± 2.3
Gd 6	53.0 ± 0.59	67.9 ± 0.34	−3.79 ± 0.26	5.63 ± 0.49	12.8 ± 1.3	6.4 ± 4.2
Gd 9	47.4 ± 0.06	48.9 ± 0.4	−4.01 ± 0.07	3.76 ± 0.13	13.5 ± 0.5	6.6 ± 2.8
Gd–DTPA[a]	51.5 ± 0.3	52.1 ± 0.6	−3.4 ± 0.1	2.60 ± 0.06	12.3 ± 0.3	4.5 ± 4.2
Gd–PCTA12[b]	30.5 ± 0.09	−11 ± 0.02	−3.01 ± 0.02	2.5 ± 0.07	13.5 ± 0.4	4.8 ± 0.8

[a]From Laurent *et al*. (28).
[b]From Port *et al*. (30).
$\Delta H_{\#}$ and $\Delta S_{\#}$ the enthalpy and entropy of activation of the water exchange process; $A/\hbar$, the hyperfine coupling constant between the oxygen nucleus of bound water molecules and the Gd_{3+} ion; B, related to the mean-square of the zero-field-splitting energy; τ_V, the correlation time modulating the electronic relaxation of Gd_{3+} and E_v, the activation energy related to τ_V.

Table 2. Relaxivity values at 20 and 60 MHz (T = 310 K) and parameters obtained from the theoretical fittings of the O-17 data and of the proton NMRD profiles of Gd(III) complexes 3, 6 and 9 and comparison with the monoaqua complex (Gd–DTPA) and the diaqua complex (Gd–PCTA12)

Compounds	r_1 at 20 MHz (s^{-1} mM^{-1})	r_1 at 60 MHz (s^{-1} mM^{-1})	τ_M[a] (ns)	τ_R (ps)	τ_{SO} (ps)	τ_V (ps)
Gd 3	5.7	5.0	35.2 ± 3.0	56 ± 1	205 ± 15	12.9 ± 3.8
Gd 6	6.4	5.7	38.5 ± 10.5	64 ± 2	194 ± 14	21.7 ± 4.1
Gd 9	6.8	6.2	42.7 ± 2.8	73 ± 1	265 ± 17	40.0 ± 1.2
Gd–DTPA[b]	3.8	3.4	143 ± 25	54 ± 1.4	187 ± 3	25 ± 3
Gd–PCTA12[c]	5.4	—	82	56	129	19

[a]Fixed parameter according to the fitting of the transverse relaxation rates of oxygen-17.
[b]From Laurent *et al*. (28).
[c]From Port *et al*. (30).

20 MHz these values are in the range 5.7–6.8 s^{-1} mM^{-1} and suggest the presence of two water molecules (q = 2) coordinated to the metal center. As a matter of fact, these values are significantly higher than those of mono-aqua Gd complexes of similar size, such as Gd–DTPA, Gd–DTPA–BMA or Gd–DOTA (3.8, 3.8 and 3.5 mM^{-1} s^{-1} at 20 MHz, respectively) (28) and are similar to those typical for *bis*-aqua Gd complexes, such as Gd–DO3A or Gd–PCTA12 (4.8 and 5.4 mM^{-1} s^{-1} at 20 MHz, respectively) (29,30). The number q was obtained by comparing the chemical shifts induced on the O-17 NMR resonance of Gd–DTPA solution (for which q = 1) and the measured values for **3**, **6** and **9**. This analysis indicated a hydration number of 2 for all studied Gd(III) complexes and thus corroborates their high relaxivities. It can be noticed that the same hydration number was established by luminescence measurements of the corresponding Eu(III) and Tb(III) complexes, on both sides of Gd(III) in the lanthanide series.

We also investigated the temperature dependence of the proton relaxivities of the three Gd complexes **3**, **6** and **9** at 20 MHz (0.47 T); such analysis reflects quantitatively the possible limitation of the global relaxivity r_1 by the residence time of the coordinated H_2O molecule (τ_M). All three complexes exhibit a continuous increase in r_1 when the temperature is lowered from 318 to 278 K (Fig. 1), revealing that τ_M does not limit the relaxation rate. At the opposite, it is well established that the global relaxivity r_1 reaches a plateau or even decreases at low temperature when τ_M is long. The quantitative evaluation of τ_M was carried out, as usual, through the analysis of the temperature dependence of the transverse relaxivity of the water oxygen-17

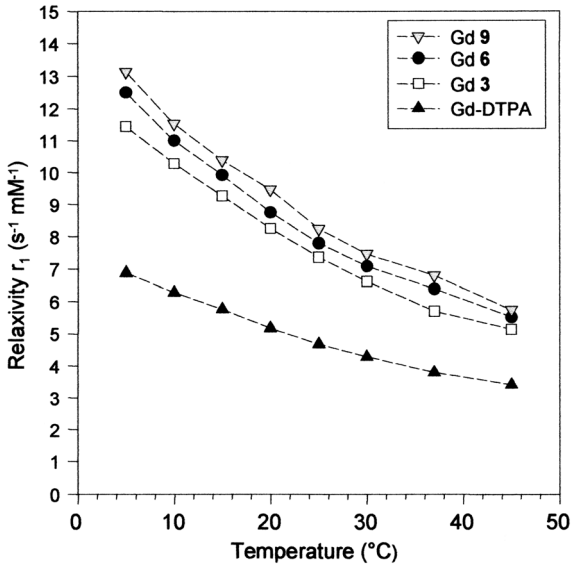

Figure 1. Temperature dependence of the proton longitudinal relaxivity of Gd(III) complexes **3**, **6** and **9** at 20 MHz (between 5 and 45 °C). Data reported for Gd–DTPA (33) are shown for comparison.

nucleus ($1/T_2^r$) in aqueous solutions of these complexes (Fig. 2). In the temperature range investigated (276–357 K), the evolution of the reduced transverse-relaxation rate of ^{17}O differs markedly from that of Gd–DTPA. Whereas the maximum of the curve for Gd–DTPA corresponds to a temperature of approximately

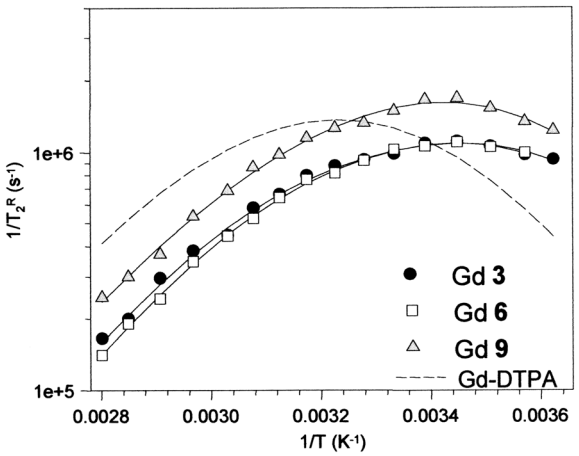

Figure 2. ^{17}O reduced transverse relaxation rate ($1/T_2^R$) as a function of the reciprocal of the temperature for aqueous solution of Gd(III) complexes **3**, **6** and **9** and Gd–DTPA. The lines correspond to the theoretical fitting of the data points.

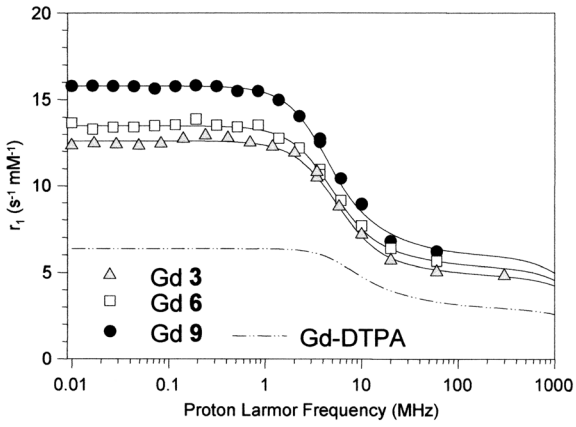

Figure 3. ^{1}H NMRD relaxivity profile of Gd(III) complexes **3**, **6** and **9** and Gd–DTPA in water at 310 K. The lines correspond to the theoretical fitting of the data points.

310 K, it is significantly shifted towards lower temperatures (range 287–297 K) for the three pyridine structures, qualitatively indicating a reduction of the residence time of the coordinated H_2O molecule. The analysis of the experimental data (between 320 and 354 K) by the appropriate theoretical model (31,32) provides a residence time of the coordinated water molecule (τ_M) in the range of 35–43 ns at 310 K (Tables 1 and 2). The presence of the extra carboxylic or amide group in **6** and **9** poorly influences the value of the exchange rate, as expected for groups that do not contribute to the coordination sphere of the metal. On the other hand, these values are three to four times shorter than that obtained for Gd–DTPA–H_2O (143 ns). They are also shorter than those reported for tetracarboxylate complexes (Gd–DOTA–H_2O, $\tau_M = 122$ ns) or tricarboxylate complexes (Gd–PCTA–$2H_2O$, $\tau_M = 82$ ns). These results are consistent with the general observation that negatively charged or *bis*hydrated species favor faster exchange (33,34). The τ_M value observed for Gd complex **6** ($\tau_M = 38.5$ ns) falls near the optimum for low imaging field (0.5 T) applications, which is in the range 10–30 ns and favors covalent coupling of this bifunctional chelate with large biomolecules (such as dendrimers, proteins or polysaccharides) for attaining an optimum relaxation enhancement (35). The fitted parameters obtained for the O-17 relaxometric data (Tables 1 and 2) are quite similar for the Gd complexes of **3**, **6** and **9** confirming the poor influence of the substitution on the pyridine on the relaxometric properties.

The longitudinal ^{1}H relaxation rates for the studied complexes were measured as a function of the magnetic field at 310 K (Fig. 3). The three Gd(III) complexes have a similar relaxivity at high magnetic field but the complex **9** is characterized by a larger low-field relaxivity, suggesting a longer electronic relaxation time at zero field (τ_{SO}). On the other hand, all three complexes have significantly higher relaxivities than Gd–DTPA over the entire magnetic field range investigated. The theoretical analysis of the NMRD profiles (Tables 1 and 2) was performed with the usual inner- and outer-sphere contributions (36). Some parameters were fixed: the number of water molecules in the first coordination sphere, q, set to the value obtained by 17-oxygen NMR ($q = 2$); the distance of closest approach, $d = 0.36$ nm; the relative diffusion coefficient D; the distance between the proton nuclei of the bound water and the gadolinium ion, $r = 0.31$ nm; and the water residence time, τ_M, fixed to the value determined by ^{17}O relaxometry. The parameters describing the rotational correlation time, τ_R, the electronic relaxation times, τ_V and τ_{SO} (the electronic relaxation time at zero field) were optimized simultaneously.

Although the set of physicochemical parameters mentioned above (r_1, q, τ_M, τ_R) provided relevant informations about the relaxometric properties of Gd(III) chelates, two other special features are usually investigated in the design of MRI contrast agents. These experiments were oriented in two directions, transmetallation with Zn^{2+} and non-covalent interaction with human serum albumin (HSA). The kinetic stability of Gd(III) complexes in the presence of Zn^{2+} ion is a stability test since the transmetallation process will induce a release of toxic free Gd(III) ion in the organism. On the other hand, it is well established that the reversible binding of Gd(III) chelates to blood proteins such as HSA, which is by far the most abundant endogenous macromolecule (0.6 mM in plasma), is a key concern for increasing their relaxivity *in vivo* and for improving their pharmacokinetics, namely longer residence lifetime in bloodstream.

The possible transmetallation process was assessed by the measurement of the evolution of the longitudinal paramagnetic relaxation rate (R_1^P) of a phosphate buffer solution containing equimolar amounts of Gd-complex and $ZnCl_2$ (2.5 mM). Transmetalation of the Gd complex by Zn^{2+} results in the release of gadolinium ions in solution. In the presence of phosphate ions, Gd ions precipitate as $GdPO_4$ and no longer contribute to the proton paramagnetic-relaxation rate of the solution. Consequently, the water proton-relaxation rate decreases, and its evolution can be used to quantitatively monitor the evolution of the system. This simple relaxometric protocol for transmetallation assessment was first developed by some of us and then applied by other research groups (37–39). In this work, we first checked that Gd chelates **3**, **6** and **9** are stable in phosphate buffer at the considered concentration (2.5 mM), pH (7) and temperature (37 °C). No significant change in relaxivity over a long period was observed for samples containing these Gd chelates only with a phosphate buffer but without Zn^{2+}. Transmetallation kinetic data are shown in Fig. 4 and are compared with those of Gd–DTPA and Gd–DTPA–BMA. This figure presents the evolution with time of the ratio of relaxation rates $R_1^P(t)/R_1^P(t_0)$, where $R_1^P(t)$ is the relaxation rate at time t and $R_1^P(t_0)$ is the relaxation rate in phosphate buffer at time zero (just before the addition of Zn^{2+}). In any case, complexes **3**, **6** and **9** are

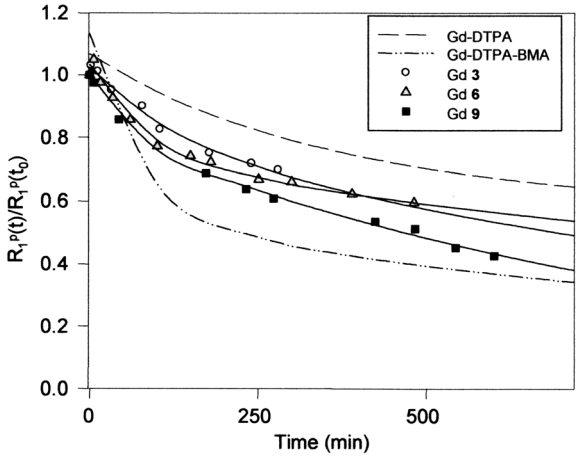

Figure 4. Transmetallation stability towards Zn^{2+}. Evolution of the ratio $R_1^p(t)/R_1^p(t_0)$ ($T = 310$ K, $B_0 = 0.47$ T, 20 MHz, pH 7.0) vs time for the Gd(III) complexes **3**, **6** and **9**, Gd–DTPA and Gd–DTPA–BMA in the presence of equimolar amounts of Zn^{2+} ions in a phosphate buffer solution.

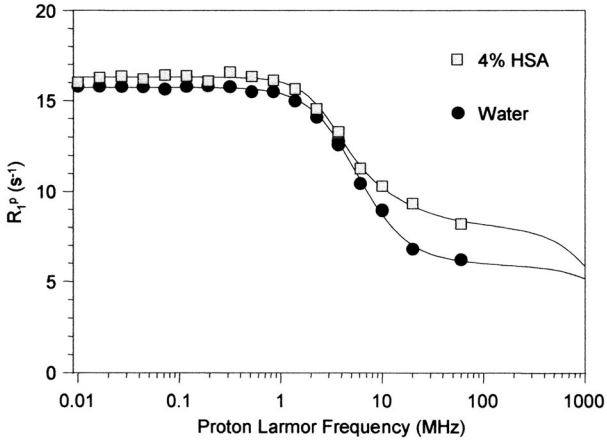

Figure 5. Relaxivity profiles of solutions containing 1 mM of complex **9** in water or in 4% HSA.

much less stable with respect to transmetallation with Zn^{2+} than the complexes with macrocyclic ligands like Gd–DOTA or Gd–PCTA12 which are inert toward this process (28,30). Their kinetic stability is comparable with those of commercial acyclic contrast agents, Magnevist and Omniscan. After 500 min, $R_1^p(t)/R_1^p(t_0)$ was of the order 50–60% for **3**, **6** and **9**, a value between those observed with Gd–DTPA (70%) and Gd–DTPA–BMA (40%). It is to be noted that our transmetallation results are quite different from those reported in Bonnet *et al*. (11) where no transmetallation was observed. This difference can be explained by the experimental conditions used in both studies and mainly by the presence of phosphate buffer in our study.

When small molecular Gd chelates interact with HSA, an increase in their rotational correlation time (τ_R), and subsequently an increase in their paramagnetic relaxation rate (R_1^p), is usually observed at magnetic fields ranging from 10 to 60 MHz (35). A convenient and nontime-consuming insight into the strength of the binding can be obtained by the measurement of R_1^p of a solution containing 1 mM of the complex in the presence of HSA (4%) at 20 MHz. An increase in this parameter larger than 60% attests to a significant interaction between the two partners (28,40). In such experiments we observed for the three complexes an increase of 20–40%, indicating that a significant interaction of the chelates with the protein can be excluded. These results were corroborated by recording the corresponding ^{1}H NMRD relaxivity profiles where no hump was observed at high fields (>10 MHz). As an example, the NMRD profile of complex **9** is shown in Fig. 5.

2.3. Luminescence studies

The UV–visible absorption spectra of the bifunctionnal Eu(III) and Tb(III) chelates **7** and **8** display a broad absorption band at 280 nm in aqueous solutions. This band attributed to π-π *transitions centered on the pyridine moiety is shifted by 5 nm toward longer wavelengths compared with that of the free ligand, indicating an electronic interaction between the light-absorbing pyridine and the light-emitting center. The room temperature emission spectra of these two visible emitting complexes show typical narrow-band lanthanide luminescence after excitation into the ligand-based pyridine π-π* absorption band. The luminescence and the corresponding excitation spectra are shown in Figs 6 and 7. The Eu(III) complex **7** is characterized by five bands in the 570–720 nm range corresponding to the $^5D_0 \rightarrow {}^7F_J$ transitions at 579 ($J = 0$), 593 ($J = 1$), 616 ($J = 2$), 651 ($J = 3$) and 696 nm ($J = 4$), with the $J = 2$ so-called 'hypersensitive' transition being the most intense. The emission spectrum of the Tb(III) complex **8** is stronger and contains four bands in the 480−630 nm range, corresponding to from the $^5D_4$ excited state to the ^7F_J ($J = 3$–6) levels centered at 489, 544, 585 and 620 nm, and the $^5D_4 \rightarrow {}^7F_5$ green emission at 544 nm is the most prominent one. It is to be noticed that both spectra of **7** and its unsubstituted counterpart **4** are similar, reflecting a constant local coordination environment around the metal ion in these complexes. This is particularly notable in the similar ratio of the integrated emission intensities for the $^5D_0 \rightarrow {}^7F_2/{}^5D_0 \rightarrow {}^7F_1$ and $^5D_0 \rightarrow {}^7F_4/{}^5D_0 \rightarrow {}^7F_1$ bands, useful parameters which may be used to assess changes in the Eu coordination environment (41). The shape and relative intensities of the terbium $^5D_4 \rightarrow {}^7F_j$ emissions in complexes **5** and **8** are also similar.

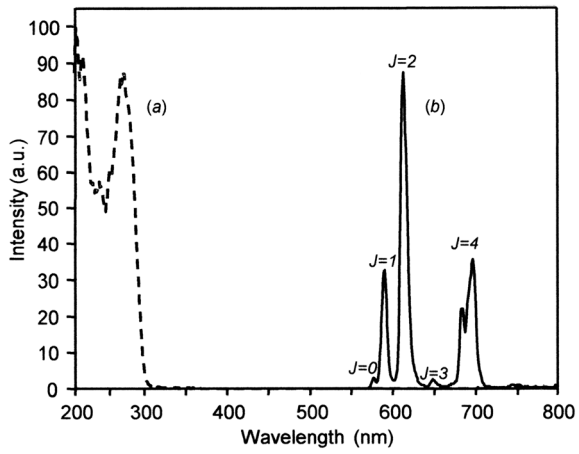

Figure 6. Corrected (*a*) excitation ($\lambda_{em} = 616$ nm) and (*b*) emission ($\lambda_{exc} = 280$ nm) spectra of the Eu complex **7** in Tris buffer at 298 K. The emission bands arise from the $^5D_0 \rightarrow {}^7F_J$ transitions; the *J* values are shown on the spectrum.

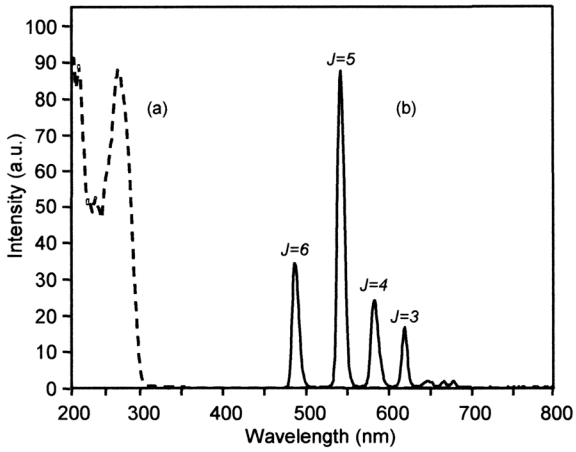

Figure 7. Corrected (*a*) excitation ($\lambda_{em} = 544$ nm) and (*b*) emission ($\lambda_{exc} = 280$ nm) spectra of the Tb complex **8** in Tris buffer at 298 K. The emission bands arise from the $^5D_4 \rightarrow {}^7F_J$ transitions; the *J* values are shown on the spectrum.

Relevant photophysical data obtained in Tris buffer (50 mM, pH 7.3) of these derivatized complexes **7** and **8** are collected in Table 3, together with analogous data for the corresponding underivatized complexes **4** and **5**. The measured luminescence lifetimes (τ_{obs}) at 298 and 77K for both complexes **7** and **8** are in the millisecond range and can be perfectly fitted with a mono-exponential function, in agreement with the presence of only one emissive Ln(III) center. From the data reported in Table 3, we can note that in D_2O solutions these lifetimes are temperature-independent, pointing to the absence of significant thermally activated deactivation pathways. Consequently, the luminescence quenching by low-lying ligand-to-metal charge-transfer states or a back-energy transfer from the metal-centered level to the ligand-centered triplet level which are commonly observed for Eu(III) and Tb(III) complexes do not occur in **7** and **8** (42). In contrast, the values of τ_{obs} measured in D_2O at room temperature were larger than in H_2O, reflecting the deactivating effect of vibrational quenching by OH oscillators, which is also revealed by the higher values for luminescence quantum yield (Φ_{obs}) in D_2O. The lower effect by solvent deuteration on terbium complex **8** ($\tau_D/\tau_H = 2.5$) relative to that observed for europium complex **7** ($\tau_D/\tau_H = 5.9$) may be rationalized by the difference of the energy gap between the lowest luminescent and the highest ground states of these lanthanide ions (43). Information about the solution hydration state *q* (which provides the number of metal-bound water molecules) of these complexes is readily available following analysis of the rate constants for radiative decays measured in light and heavy water. Using the well-known expressions developed by Horrocks *et al.* and Parker *et al.*, taking into account the quenching contribution of closely diffusing (second sphere) water molecules (44,45), the hydration state values obtained for these Eu(III) and Tb(III) complexes are in good agreement with another, at 2.0 in each case. In connection with the UV data, this result indicates that ligand **2** acts as a heptadentate ligand in the complexation of Ln(III) ions: four carboxylate oxygens and two nitrogens in the iminodiacetic backbones and pyridine nitrogen. The luminescence quantum yields (Φ_{obs}) which take into account the efficiency of the overall energy-transfer process from the pyridine sensitizer to the lanthanide ion are modest ($\leq$ 10%), but much larger than those reported by Bonnet *et al.* (11) and fully remain within the actual range of commercially available di-aqua complexes (46,47).

In the luminescent process of sensitized Eu(III), Tb(III) chelates (48), an important parameter to be considered is the triplet state energy of the ligand centered levels under the perturbation caused by coordination to a paramagnetic ion. This was measured as usual from the ligand phosphorescence spectrum of the corresponding Gd complex. Upon UV excitation at 77 K, the emission spectrum of **6** showed a broad band extending from 350 to 550 nm, with an apparent maximum at 407 nm and lifetime of 24 ms. This value allowed us to estimate that in **7** and **8** the ligand triplet state lies above 24550 cm^{-1}, and thus energy transfer to Eu(III) is feasible to its $^5D_2$, $^5D_1$, $^5D_0$ levels ($\Delta E = 3050$, 5550 and 7250 cm^{-1}, respectively) and to Tb (III) through its $^5D_4$ level ($\Delta E = 4050$ cm^{-1}). We can also note that this triplet state energy appears only slightly bathochromically shifted ($\Delta E = 600$ cm^{-1}) in comparison with that of the parent complex **3**. Another parameter of interest, in designing ligands able to generate efficient antenna effect is the sensitization efficiency η_{sens}, which stands for the efficiency of the intersystem crossing process of the antenna ($^1\pi\pi^* \rightarrow {}^3\pi\pi^*$) and for the efficiency of the energy

Table 3. Photophysical data of Eu(III) and Tb(III) complexes in aerated Tris-buffer (50 mM, pH 7.4) at 298 K

Chelate	$\lambda_{abs\ max}$ (nm)	ε ($dm^3\ mol^{-1}\ cm^{-1}$)	τ_{obs} (H_2O) (ms)	τ_{obs}[a] (D_2O) (ms)	Φ_{obs}[b] (H_2O) (%)	q_{H2O}[c]	$E^3\pi\pi^*$[d] (cm^{-1})
Eu 4	267	3400	0.40	2.35	2.8	2	25150
Tb 5	267	3300	1.26	3.13	8.5	2	25150
Eu 7	280	3150	0.39	2.29 (2.35)	3 (21)	2	24550
Tb 8	280	3200	1.22	3.06 (3.18)	10 (26)	2	24550
Tb 10	273	4400	1.24	2.99	4 (11.2)	2	—

[a]Lifetimes at 77 K in parentheses.
[b]Quantum yields in D_2O in parentheses.
[c]Number of metal coordinated water molecules at 298K, calculated using the Horrocks equation (44) (Eu complexes) and the Parker equation (45) (terbium complexes).
[d]Energetic position of the ligand first excited triplet state, determined from phosphorescence data of the corresponding Gd(III) complexes in frozen solutions at 77 K, in a EtOH–MeOH (1:4) mixture.

transfer from the antenna-centered to the metal-centered excited states ($^3\pi\pi^* \rightarrow Ln^*$) (49). This quantity can be estimated from equation (1):

$$\eta_{sens} = \Phi_{obs}/\Phi_{Ln} = \Phi_{obs} \times \tau_{Ln}/\tau_{obs} \quad (1)$$

where Φ_{obs} and τ_{obs} are the luminescence quantum yield and lifetime determined experimentally upon excitation into the singlet state of the antenna, and Φ_{Ln} and τ_{Ln} the luminescence quantum yield and lifetime determined upon direct f–f excitation (so-called intrinsic quantum yield and radiative lifetime, respectively). In the case of Eu(III) complexes and following the relationship developed by Werts *et al*. (50), it was possible to calculate the radiative lifetime of europium (τ_{Eu}) from the corrected emission intensities of the entire spectrum and of the magnetic-dipole $^5D_0 \rightarrow {}^7F_1$ ($I_{\Sigma FJ}$ and I_{F1}, respectively), the refractive index of the solution (n) and eqn (2):

$$1/\tau_{Eu}(s^{-1}) = 14.65 \times n^3 \times I_{\Sigma FJ}/I_{F1} \quad (2)$$

For europium complexes **4** and **7** the results of these calculations [eqns (1) and (2)] lead to the values of τ_{Eu}, Φ_{Eu} and η_{sens} given in Table 4. As expected, Φ_{Eu} changes significantly (6-fold) on going from H_2O to D_2O, but not the sensitization efficiency (η_{sens}), which is independent of the presence of inner sphere water molecules. This η_{sens} parameter is sizeable (30–40%) and can be compared favorably with the value of 43% calculated for the 12-membered polyaza-macrocyclic ligand incorporating a diethylenetriacetic core and an intracyclic pyridine moiety (Eu·PCTA[12]) (51). The main factor that limits the observed luminescence quantum yield is the rather low efficiency of metal-centered luminescence. With regard to the influence of ligand structure on the luminescence efficiency of europium complexes, we notice that the introduction of a *para*-carboxylic acid group at the pyridine ring in going from **4** to **7** provides a batochromic shift of the π–π^* absorption band (13 nm) but does not significantly alter the luminescence properties. The substitution has a small effect on the experimental photophysical properties (τ_{obs}, Φ_{obs}), the intrinsic photophysical properties of europium (τ_{Eu}, Φ_{Eu}) or the ligand-to-metal energy transfer (η_{sens}). It is noteworthy that values of both τ_{Eu} and Φ_{Eu} are very close for **4** and **7**, reflecting a similar coordination environment of Eu(III) in both complexes.

When compared with the photophysical properties of the corresponding free luminescent bifunctional label **8**, the maxima and the shape of excitation and emission spectra of the bioconjugate Tb(III) chelate **10** remain unchanged. Moreover, the luminescence lifetime and the hydration number ($q = 2$) of **10** indicate that no replacement of metal-bound water molecules by coordinating groups from the peptide core is effective. This result is in agreement with the relaxometric experiments.

As far as the stability of these complexes is concerned (Fig. 8), the emission properties of Eu(III) complex **7** in aerated solution remained unchanged for several days in Tris buffer at pH 7.3. The same stability, lifetime and quantum yield of this complex were obtained in other common buffers used in biology (HEPES buffer pH 7.3, phosphate buffer pH 7.3 and borate buffer pH 8.6). Interestingly, the absence of changes in the form of the emission spectrum, total intensity and lifetime of **7** in phosphate buffer is consistent with the retention of the two coordinated water molecules in the presence of this potential mono- and bidentate anion. A series of experiments was also undertaken to assess the inertness of this complex to the presence of bidentate oxy-anions of biological relevance as L-lactate, citrate, carbonate or bicarbonate. As a matter of fact, it has been shown by luminescence emission studies that diaqua lanthanide complexes with heptadentate ligands, such as macrocyclic DO3A derivatives, form ternary adducts with these chelating dianions (10-fold excess), in which displacement of both of the metal-bound water molecules occurs (52,53). Addition of a same excess of these dianions (Tris buffer, pH 7.3) caused no change in the emission properties (τ_{obs} and Φ_{obs}) of complex **7**, indicating that this process does not occur. These results are probably due to the negative charge of the complex and to the arrangement of the two first-shell water molecules (54). The complex is less stable with respect to acid-catalyzed dissociation pathway: at pH 2, 75% dissociation was observed after 24 h. On the other hand, the total emission intensity and emission lifetime exhibited no variation at pH 12, suggesting the absence of deprotonation of the coordinated water molecules. These experiments are illustrated in Fig. 8. Parallel series of experiments were undertaken with Tb complex **8** and led to similar results: high kinetic stability in various aqueous buffers and inertness towards bidentate di-anion.

Table 4. Calculated values of τ_{Eu}, Φ_{Eu} and η_{sens} for Eu(III) complexes **4** and **7** using experimentally determined quantities τ_{obs}, Φ_{obs} and $[I_{F1}/I_{\Sigma F0\text{-}4}]$ in Tris-buffer (pH 7.4) at 298 K

	Eu 4 (H_2O)	**Eu 7** (H_2O)	**Eu 7** (D_2O)
$[I_{F1}/I_{\Sigma FJ}]$	0.156	0.152	0.150
τ_{Eu} (ms)	4.52	4.41	4.35
τ_{obs} (ms)	0.40	0.39	2.29
Φ_{Eu} (%)	0.09	0.09	0.53
Φ_{obs} (%)	0.028	0.03	0.21
η_{sens} (%)	0.31	0.33	0.40

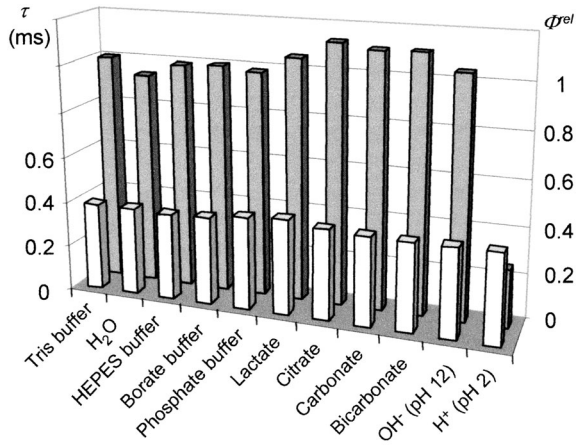

Figure 8. Eu lifetimes (white) and Eu relative quantum yields Φ^{rel} (gray) of complex **7** in various buffers (Tris pH 7.4, HEPES pH 7.3, phosphate pH 7.3, borate pH 8.6), in the presence of the stated additives (16 μM complex, 160 μM additive, Tris buffer pH 7.4), in NaOH (0.01 M pH 12) and HCl solutions (0.01 M pH 2). Arbitrarily, the value of the quantum yield of **7** in Tris buffer was taken as 1.

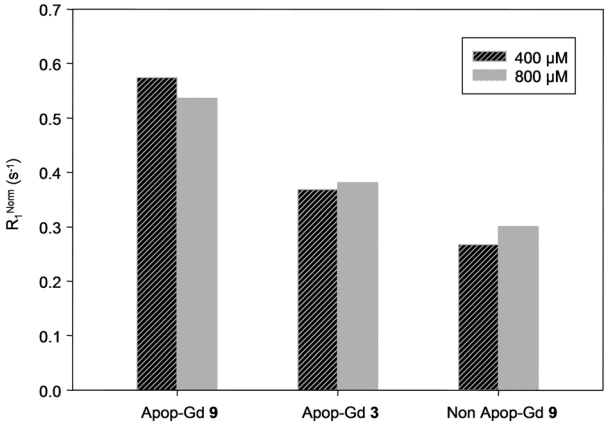

Figure 9. Normalized R_1 ($R_1^{norm} = R_1^{obs} - R_1$ of untreated cells) of 2×10^6 apoptotic transplantable liver tumor cells or of control cells incubated with 400 µM and 800 µM of Gd **3** or Gd **9** at 20 MHz.

2.4. Test on cell culture

As a proof of concept, the specificity of the Gd complex **9** for apoptotic cells was tested. Apoptosis was induced on transplantable liver tumor cells [mouse hepatocarcinoma, kind gift from Professor O. Feron (UCL, Pole of Pharmacology)] by incubation with camptothecin 1 µM during 24 h. Two million cells were then incubated with Gd **3** or Gd **9** at two concentrations (400 and 800 µM) during 2 h. After centrifugation, removal of the supernatant and washing, cells were then resuspended in gelatine (2%) and the T_1 was measured at 20 MHz and 25 °C. The cell model that was used in the preliminary biological experiments was a model of cell death (induced apoptosis). The attempt consisted in the targeting of cell surface-exposed phosphatidylserine in the death process. Thus, at such a preliminary stage, we did not *a priori* work with the aim of getting the compound internalized by cells and quantifying it. In *in vitro* cellular labeling contexts it is a desired mechanism of contrast agent accumulation in the cell for better labeling and subsequent MRI detection of cells (e.g. when implanted in the body). Aime *et al*. published several reports about the phenomenon of pinocytosis that allows Gd chelates to enter cells (55). In the case of cell surface targeting, it may be supposed that endocytosis of the compound can also occur subsequently to its interaction with the target on the cell surface, possibly as a desired mechanism of contrast accumulation for better MRI detection.

The paramagnetic contribution to R_1 is markedly increased for apoptotic cells incubated with Gd **9** as compared either with Gd **3** (40–56%) or with control cells incubated with Gd **9** (78–115%; Fig. 9). No significant difference was observed between the two concentrations of the Gd complexes. These data confirm that Gd **9** specifically labels the apoptotic cells.

3. CONCLUSIONS

A 4-carboxylic acid substituted pyridine derivative (**2**) of PMN-tetraacetic acid moiety {PMN-tetraacetic acid (**1**): [2,6-pyridinediyl*bis*(methylene nitrilo)-tetraacetic acid]}, was synthesized and complexed with Ln(III) ions (Ln = Gd, Eu, Tb). These complexes have two water molecules in the inner coordination sphere of the metal. The Gd complex shows a high proton relaxivity ($r_1 = 6.4$ s^{-1} mM^{-1} at 20 MHz) with short water residence time ($\tau_M = 38.5$ ns) whereas the terbium complex has a luminescence lifetime of 1.22 ms at room temperature and a luminescence quantum yield of 10%. These complexes are characterized by a good kinetic stability in medium containing blood proteins, cations or bioactive oxyanions and the Gd complex does not interact with HSA, but undergoes a transmetalation reaction with Zn(II) in a phosphate buffer solution (pH 7.4), rather similar to that of Gd–DTPA–BMA(H_2O). On the other hand, Eu and Tb complexes do not form ternary complexes with bidentate anions such as L-lactate, citrate or carbonate. The gadolinium and terbium complexes show thus promising properties either for MRI or optical imaging. Finally, a phosphatidylserine-specific hexapeptide (TLVSSL) was grafted on both Gd or Tb chelates. The potential *in vitro* targeting of the Gd–peptide conjugate for apoptotic cells was confirmed by a relaxometric study of apoptotic cells incubated with this complex.

4. EXPERIMENTAL

4.1. General procedures

Column chromatography was carried out on silica gel (Merck, 60–200 µm, porosity 60 Å) and on alumina (Macherey-Nagel, activity IV, 50–200 µm). Melting points were taken with a Büchi mel-temp apparatus. Infrared spectra were recorded as thin films on sodium chloride plates using a Perkin-Elmer FTIR 1725× spectrophotometer. Selected characteristic absorption frequencies are reported in cm^{-1}. ^1H and ^{13}C NMR spectra were recorded on a Bruker Avance 300 spectrometers; chemical shifts are given in ppm according to the solvent peak and *J* values are given in Hz. Low-resolution mass spectrometry was carried out on a Q TRAP Applied Biosystems Spectrometer (ESI^+). HRMS was performed using a Q-tof Ultima (Waters). Absorption measurements were done with a Hewlett Packard 8453 temperature-controlled spectrophotometer. The analytical HPLC was performed on a Waters–Acquity system equipped with PDA detector and using an Acquity UPLC BEH HILIC column (1.7 µm, 2.1 × 100 mm). The compounds were analyzed using as HPLC isocratic system a mixture of 10% of ammonium formate buffer (10 mM, pH 4) in CH_3CN (85%) and ammonium formate buffer (10 mM, pH 4; 15%) at a flow rate of 0.6 ml min^{-1} and with UV monitoring at 273 nm.

4.2. NMR measurements

^{17}O NMR measurements were recorded at 7.05 T on a Bruker AMX-300 spectrometer (Bruker, Karlsrhue, Germany). The number of coordinated water molecules (*q*) in the Gd-complex was determined by the O-17 chemical shift of water resonance. ^{17}O NMR measurements at natural abundance were performed on 2 ml samples contained in 10 mm o.d. tubes. ^{17}O diamagnetic transverse-relaxation times of water were measured using the CPMG sequence (90 and 180° pulse lengths were 25 and 50 µs, respectively). All ^{17}O NMR spectra were proton decoupled. ^{17}O transverse-relaxation times of water in solutions containing the Gd complex were calculated from the spectral line width. The temperature was controlled by a BVT-2000 unit. The concentrations used for these studies are 21.55 mM for Gd complex **3**, 24.95 mM for Gd complex **6** and 8.058 mM for Gd complex **9**.

Measurements of the longitudinal relaxation rates at 0.47 T were performed on a Minispec mq-20 (Bruker, Karlsrhue,

Germany) temperatures ranging from 5 to 45 °C and on a fast field cycling relaxometer Stelar (PV, Mede, Italy) at 37 °C. Additional relaxation rates at 0.47 and 1.4 T were obtained on a Minispec mq-20 and mq-60, respectively (Bruker, Karlsruhe, Germany). Fitting of the ^{1}H NMRD was performed with data-processing software using different theoretical models describing the nuclear-relaxation phenomena observed (Minuit, CERN Library) (56). The final concentration of the gadolinium complex solution was determined by proton relaxometry at 0.47 T.

Transmetalation by zinc ions was evaluated by the decrease of the water longitudinal relaxation rate at 37 °C and 20 MHz (Bruker Minispec mq-20) of buffered phosphate solutions (pH 7, $[KH_2PO_4]$ 0.026 mol l^{-1}, $[Na_2HPO_4]$ 0.041 mol l^{-1}) containing 2.5 mM gadolinium complex and 2.5 mM Zn (57).

4.3. Photophysical measurements

Fluorescence and phosphorescence spectra were obtained with a LS-50B Perkin-Elmer and a Cary Eclipse spectrofluorimeters equipped with a xenon flash lamp source and a Hamamatsu R928 photomultiplier tube. The measurements were carried out at pH 7.4 in Tris buffer (50 mM) and all samples were prepared with an absorbance between 0.01 and 0.05 at the excitation wavelength in order to prevent the inner-filter effect. Phosphorescence spectra at 77 K of gadolinium complexes were carried out in a MeOH–EtOH (4:1 v/v) mixture and recorded with the LS-50B Perkin-Elmer spectrofluorimeter equipped with the low-temperature accessory no. L2250136. Spectra were corrected for both the excitation light source variation and the emission spectral response. Lifetimes (uncertainty ≤ 5%) are the average values from at least five separate measurements covering two or more lifetimes made by monitoring the decay at a wavelength corresponding to the maximum intensity of the emission spectrum, following pulsed excitation. The luminescence decay curves were fitted by an equation of the form $I(t) = I(0)\exp(-t/\tau)$ by using a curve-fitting program. The number of metal coordinated water molecules at 298 K, calculated using the following equations: $q_{H2O}(Eu) = 1.11[(\tau_{H2O})^{-1} - (\tau_{D2O})^{-1} - 0.31]$ (44) and $q_{H2O}(Tb) = 5[(\tau_{H2O})^{-1} - (\tau_{D2O})^{-1} - 0.06]$ (45). The luminescence quantum yields (uncertainty ± 15%) were calculated by using the following equation:

$$\Phi/\Phi_r = [A_r(\lambda_r)/A(\lambda)][I/I_r]\left[n^2/n_r{}^2\right]$$

where A, I and n denote the absorbance at the excitation wavelength (λ), the integrated luminescence intensity, and the refractive index of solvent, respectively. Subscript 'r' denotes the reference, and no subscript denotes the unknown sample. Quinine sulfate in 1 M sulfuric acid (Φ = 0.546) and $[Ru(bpy)_3]^{2+}$ in aerated water (Φ = 0.028) were used as the references for the Tb(III) and Eu(III) complexes, respectively (58,59).

4.4. 1-Methoxy-2,6-dimethylpyridinium methyl sulfate (11)

Dimethyl sulfate (19.2 g, 0.152 mol) was added portionwise to 2,6-lutidine-1-oxyde (18.7 g, 0.152 mol). The temperature of the reaction mixture was maintained at 80 °C during the addition. After the addition was complete, the solution was heated at 80 °C for 3 h. The reaction mixture was cooled to room temperature and the precipitate was recrystallized in acetone yielding **11** (33 g, 87%) as colorless crystals. R_f: 0.38 (silica, methanol). FT-IR (KBr): ν_{max}/cm^{-1} 1266 (OSO_3^-). ^{1}H NMR (300 MHz, DMSO-d_6): δ 2.76 (s, 6H), 3.29 (s, 3H), 4.22 (s, 3H), 7.90 (d, 2H, J = 7.8), 8.29 (t, 1H, J = 7.8). ^{13}C NMR (75 MHz, DMSO-d_6): δ 17.4 (CH_3), 53.5 (CH_3), 67.5 (CH_3), 128.6 (CH), 144.4 (CH), 153.6 (C_q).

4.5. 4-Cyano-2,6-dimethylpyridine (12)

To a solution of **11** (33 g, 0.133 mol) in water (35 ml) was added dropwise a solution of potassium cyanide (25.9 g, 0,400 mol) in water (55 ml) and the resulting suspension was stirred at room temperature under argon for 4 days. The pink precipitate was removed by filtration and the filtrate was extracted with diethylether (3 × 50 ml). The combined organic solutions were dried over $MgSO_4$ and concentrated under vacuum. The resulting residue and the pink precipitate obtained above were purified by using column chromatography on silica gel (dichloromethane) to yield **12** as a white powder (5.8 g, 33%). R_f: 0.22 (silica, dichloromethane). FT-IR (KBr): ν_{max}/cm^{-1} 2235 (CN). ^{1}H NMR (300 MHz, $CDCl_3$): δ 2.58 (s, 6H), 7.18 (s, 2H). ^{13}C NMR (75 MHz, $CDCl_3$): δ 24.3 (CH_3), 118.8 (C_q), 120.9 (C_q), 121.9 (CH), 159.4 (C_q).

4.6. 2,6-Dimethylpyridine-4-carboxylic acid methyl ester (13)

A mixture of **12** (0.5 g, 3.78 mmol), sodium hydroxide (2.5 M, 3 ml), ethanol (3 ml) was reacted at 100 °C for 5 h. After cooling to room temperature, the solution was concentrated under vacuum and was acidified to pH 3 with 10% hydrochloric acid. After evaporation to dryness, 2,6-dimethylisonicotinic acid (1.1 g) was obtained as a white solid and was used without purification for the next step. FT-IR (KBr): ν_{max}/cm^{-1} 3330 (OH), 1697 (C=O acid). ^{1}H NMR (300 MHz, $CDCl_3$): δ 2.62 (s, 6H), 7.76 (s, 2H). ^{13}C NMR (75 MHz, D_2O): δ 18.9, 122.8, 148.9, 154.7, 167.9. A mixture of 2,6-dimethylisonicotinic acid (1.1 g) and 98% sulfuric acid (0.75 ml) in methanol (75 ml) was heated at reflux for 24 h. After cooling to room temperature, the resulting solution was neutralized with an aqueous saturated solution of $NaHCO_3$. Methanol was removed under vacuum and the aqueous layer was extracted with dichloromethane (5 × 60 ml). The combined organic layers were dried over $MgSO_4$ and concentrated under vacuum. The resulting residue was purified using column chromatography on silica gel (dichloromethane–ethyl acetate, 8:2) to yield **13** as a white powder (0.49 g, 78%). R_f: 0.52 (silica, dichloromethane–ethyl acetate, 7:3). FT-IR (KBr): ν_{max}/cm^{-1} 1723 (C=O ester). ^{1}H NMR (300 MHz, $CDCl_3$): δ 2.53 (s, 6H), 3.87 (s, 3H), 7.45 (s, 2H). ^{13}C NMR (75 MHz, $CDCl_3$): δ 24.5 (CH_3), 52.5 (CH_3), 119.5 (CH), 137.9 (C_q), 158.9 (C_q), 166.2 (C_q).

4.7. 2,6-*Bis*(hydroxymethyl)pyridine-4-carboxylic acid methyl ester (15)

A stirred solution of methylisonicotinate (540 mg, 3.94 mmol) in methanol (20 ml) with concentrated H_2SO_4 (50 µl) was heated at 90 °C, then a solution of ammonium persulfate (9 g, 39.4 mmol) in water (20 ml) was added dropwise, and the reaction mixture was refluxed for 1 h. Methanol was removed under vacuum and the aqueous layer was neutralized with an aqueous saturated solution of $NaHCO_3$, then extracted with dichloromethane (4 × 50 ml). The combined organic layers were dried over $MgSO_4$ and concentrated under vacuum. The resulting residue was purified by using column chromatography on silica gel (ethyl acetate) to yield **15** as a yellow solid (534 mg, 68%). m.p

125–126 °C. R_f: 0.33 (silica, ethyl acetate). FT-IR (KBr): ν_{max}/cm^{-1} 3541 (OH), 1711 (C = O ester). ^1H NMR (300 MHz, $CDCl_3$): δ 3.96 (s, 3H), 4.84 (s, 4H), 7.77 (s, 2H). ^{13}C NMR (75 MHz, $CDCl_3$): δ 52.9 (CH_3), 64.5 (CH_2), 118.7 (CH), 138.9 (C_q), 160.1 (C_q), 165.5 (C_q). MS (ESI^+): *m/z* 220.0 $[M + Na]^+$, 198.1 $[M + H]^+$.

4.8. 2,6-*Bis*(bromomethyl)pyridine-4-carboxylic acid methyl ester (14)

*4.8.1. From 2,6-dimethylpyridine-4-carboxylic acid methyl ester (**13**)*

A mixture of **13** (2.96 g, 17.93 mmol), NBS (6.38 g, 35.86 mmol) and benzoylperoxide (100 mg) in CCl_4 (200 ml) was refluxed under diazote and lightened using a halogen lamp (150 W). The mixture was allowed to stir for 2 h upon which the solution decolorized. Then more NBS (5.18 g, 29.11 mmol) was added, and the reaction mixture was allowed to stir at reflux for another 5 h 30 min. After cooling to room temperature, the resulting solution was neutralized with an aqueous saturated solution of $NaHCO_3$ (100 ml), and extracted with dichloromethane (3 × 50 ml). The combined organic layers were dried over $MgSO_4$ and concentrated under vacuum. The resulting residue (orange solid), a mixture of polybrominated products, was dissolved in dry THF (70 ml) and placed in an ice bath under argon atmosphere. Diisopropylethylamine (13.8 ml, 79 mmol) was added followed by dropwise addition of diethylphosphite (10.2 ml, 79 mmol), and the resulting solution was stirred at 0 °C for 30 min then stirred at room temperature for 18 h. Ice water (100 ml) was added and the aqueous layer was extracted with diethylether (3 × 50 ml). The combined organic layers were dried over $MgSO_4$ and concentrated under vacuum. The resulting residue (brown oil) was purified using column chromatography on silica gel (dichloromethane–petroleum etherm 1:1) to yield **14** as a white powder (3,3 g, 57%).

*4.8.2. From 2,6-bis(hydroxymethyl)pyridine-4-carboxylic acid methyl ester (**15**)*

The diol **15** (100 mg, 0.51 mmol) was treated with PBr_3 (80 µl, 0.85 mmol) in dry chloroform (2 ml) at reflux for 20 h. The reaction mixture was cooled at room temperature and quenched with an aqueous saturated solution of $NaHCO_3$. Layers were separated and the aqueous layer was extracted with dichloromethane (4 × 15 ml). All the organic layers were combined and dried over $MgSO_4$, and concentrated under vacuum. The resulting residue (beige solid) was purified by using column chromatography on silica gel (dichloromethane–petroleum ether, 6:4) to yield **14** as a white solid (99 mg, 61%); m.p. 92 °C [literature 90–92 °C (20)]. R_f: 0.32 (silica, dichloromethane–petroleum ether, 1:1). FT-IR (KBr): ν_{max}/cm^{-1} 1721 (C = O ester). ^1H NMR (300 MHz, $CDCl_3$): δ 3.97 (s, 3H), 4.58 (s, 4H), 7.92 (s, 2H). ^{13}C NMR (75 MHz, $CDCl_3$): δ 32.9 (CH_2), 53.0 (CH_3), 122.3 (CH), 139.8 (C_q), 158.0 (C_q), 164.8 (C_q). MS (DCI, NH_3): *m/z* 323.9 $[M + H]^+$.

4.9. Tetra(*tert*-butyl)2,2′,2″,2‴[4-(methoxycarbonyl) pyridine-2,6-diyl]*bis*(methylenenitrilo)-tetrakis (acetate) (16)

Na_2CO_3 (7 g, 66 mmol) was added to a solution of di*tert*butyiminodiacetate (3 g, 12.24 mmol), 2,6-*bis* (bromomethyl)pyridine-4-carboxylic acid methyl ester **14** (2 g, 6.19 mmol) in anhydrous acetronitrile (450 ml). The suspension was refluxed under argon for 16 h. After the mixture was cooled to room temperature, the insoluble solid was filtered off. The solvent was evaporated under reduced pressure and the residue was purified using column chromatography on alumina (dichloromethane–petroleum ether, 7:3 → 1:0) to yield **16** as a pale yellow oil solid (3.47 g, 86%). R_f: 0.40 (alumina, dichloromethane). ^1H NMR (300 MHz, $CDCl_3$): δ 1.45 (s, 36H), 3.48 (s, 8H), 3.91 (s, 3H), 4.08 (s, 4H), 8.03 (s, 2H). ^{13}C NMR (75 MHz, $CDCl_3$): δ 28.1 (CH_3), 52.4 (CH_3), 55.8 (CH_2), 59.5 (CH_2), 81.0 (C_q), 120.3 (CH), 138.7 (C_q), 160.1 (C_q), 166.1 (C_q), 170.3 (C_q). MS (ESI^+): *m/z* 674.5 $[M + Na]^+$, 652.5 $[M + H]^+$.

4.10. 2,2′,2″,2‴-[(4-carboxy)pyridine-2,6-diyl)*bis* (methylenenitrilo)]-tetrakis (acetic acid) (2)

The pentaester **16** (1.51 g, 2.32 mmol) was stirred in a 6 M HCl solution (50 ml) at 90 °C for 2 days. After cooling to room temperature, the solution was washed with diethylether (25 ml), and the aqueous layer was evaporated under reduced pressure to give **2** in the form of its trishydrochloride salt as a white solid (1.24 g, 100%). ^1H NMR (300 MHz, D_2O): δ 4.24 (s, 8H), 4.79 (s, 4H), 8.02 (s, 2H). ^{13}C NMR (75 MHz, D_2O): δ 55.3 (CH_2), 58.6 (CH_2), 125.2 (CH), 141.7 (C_q), 150.8 (C_q), 166.9 (C_q), 168.5 (C_q). MS (ESI^+): *m/z* 436.3 $[M + Na]^+$; 414.3 $[M + H]^+$. Analysis calculated for $C_{16}H_{19}N_3O_{10}3HCl{\cdot}H_2O$: C, 35.54; H, 4.47; N, 7.77%. Found: C, 35.72; H, 4.62; N, 7.68%. λ_{max} (Tris buffer, pH 7.4)/nm 275 (ε/dm^3 mol^{-1} cm^{-1} 3150).

4.11. Ln(III) chelates 3–8

4.11.1. General procedure

To a water solution of the tetraacetic acids **1** or **2** was added $LnCl_3.6H_2O$ salt (Ln = Eu, Tb, Gd 1.1 equiv.) in water at room temperature while maintaining the pH at 7.4 with an NaOH solution. The resulting mixture was then stirred for 24 h at room temperature and passed through Chelex-100 to trap free Ln^{3+}, and the Ln^{3+}-loaded complex was recovered. The solvent was removed, the resulting solid was dissolved in a minimum of MeOH and Et_2O was added to precipitate the desired complex, which was isolated by centrifugation and dried under vacuum. Arsenazo test confirmed the absence of free lanthanide ions and the absence of free ligand was confirmed by mass spectrometry. The solutions of the complexes were used without further purification.

*4.11.2. Gd(III) chelate **3***

MS (ESI^-): *m/z* 523.0 ($[M - H]^-$), λ_{max} (Tris buffer, pH 7.4)/nm 267 (ε/dm^3 mol^{-1} cm^{-1} 3400).

*4.11.3. Eu(III) chelate **4***

MS (ESI^-): *m/z* 518.1 ($[M - H]^-$), λ_{max} (Tris buffer, pH 7.4)/nm 267 (ε/dm^3 mol^{-1} cm^{-1} 3400), λ_{em} (Tris buffer, pH 7.4, λ_{exc} = 267 nm)/nm 580 (relative intensity, corrected spectrum 2), 593 (32.4), 616 (100), 652 (3.5) and 700 (69.3).

*4.11.4. Tb(III) chelate **5***

MS (ESI^-): *m/z* 524.0 ($[M - H]^-$), λ_{max} (Tris buffer, pH 7.4)/nm 267 (ε/dm^3 mol^{-1} cm^{-1} 3300), λ_{em} (Tris buffer, pH 7.4, λ_{exc} = 267 nm)/nm 489 (relative intensity, corrected spectrum 39.2), 544 (100), 584(31.1) and 621 (15.4).

4.11.5. *Gd(III) chelate* **6**

MS (ESI$^-$): *m/z* 567.2 ([M − H]$^-$), λ_{max} (Tris buffer, pH 7.4)/nm 280 (ε/dm^3 mol^{-1} cm^{-1} 3500).

4.11.6. *Eu(III) chelate* **7**

MS (ESI$^-$): *m/z* 562.1 ([M − H]$^-$), λ_{max} (Tris buffer, pH 7.4)/nm 280 (ε/dm^3 mol^{-1} cm^{-1} 3150), λ_{em} (Tris buffer, pH 7.4, λ_{exc} = 280 nm)/nm 579 (relative intensity, corrected spectrum 1.8), 593 (30.9), 616 (100), 651 (3.3) and 696 (67).

4.11.7. *Tb(III) chelate* **8**

MS (ESI$^-$): *m/z* 568.0 ([M − H]$^-$), λ_{max} (Tris buffer, pH 7.4)/nm 280 (ε/dm^3 mol^{-1} cm^{-1} 3200), λ_{em} (Tris buffer, pH 7.4, λ_{exc} = 280 nm)/nm 489 (relative intensity, corrected spectrum 38.8), 544 (100), 585 (31.2) and 620 (15.8).

4.12. Peptide chelates 9 and 10

4.12.1. *General procedure*

Gadolinium (**6**) or terbium (**8**) complexes (49.9 μmol) in H_2O (1 ml) were stirred with *N*-hydroxysulfosuccinimide sodium salt (15 mg, 69 μmol) and EDCI.HCl (11 mg, 57.4 μmol) at room temperature for 24 h. Peptide (38.1 mg, 49.9 μmol) was then added and the mixture was stirred for further 48 h. The reaction mixture was then dialyzed (cut-off of the membrane 1000, spectra-Por, VWR, Leuven, Belgium).

4.13. Gd(III) chelate 9

56% yield. Analytical HPLC: t_R = 1.71 min; HRMS (ESI$^+$): *m/z* ([M + H]$^+$), calculated for $C_{49}H_{74}N_{10}GdNa_2O_{22}$, 1358.401565; found, 1358.4029; λ_{max} (Tris buffer, pH 7.4)/nm 273 (ε/dm^3 mol^{-1} cm^{-1} 4400).

4.13.1. *Tb(III) chelate* **10**

54% yield. Analytical HPLC: t_R = 1.71 min; HRMS (ESI$^+$): *m/z* ([M + H]$^+$), calculated for $C_{49}H_{74}N_{10}TbNa_2O_{22}$, 1359.402804; found, 1359.4030. λ_{max} (Tris buffer, pH 7.4)/nm 273 (ε/dm^3 mol^{-1} cm^{-1} 4400); λ_{em} (Tris buffer, pH 7.4, λ_{exc} = 283 nm)/nm 489 (relative intensity, corrected spectrum 38.5), 544 (100), 584 (30.1) and 621 (15.2).

4.14. Cell cultures

Transplantable liver tumor cells were cultured in DMEM [Dulbeccos's modified Eagle's medium (high glucose with GlutaMAX™); reference number 61965 from Invitrogen, Merelbeke, Belgium] completed with 10% fetal bovine serum and 1% antibiotic–antimycotic (Invitrogen). They were collected in 5 ml of medium for counting. Two milion cells were incubated during 2 h at room temperature in 1 ml of medium containing the contrast agent. For washings, cells were centrifuged (15 min at 8000 rpm, room temperature) and the cell pellet was then resuspended in 500 μl of a calcium-containing buffer (similar to Annexin V binding buffer) and centrifuged again (15 min at 8000 rpm). This step was repeated three times. The cell pellet was finally resuspended in 200 μl of gelatin 2% prepared in the calcium-containing buffer.

Acknowledgments

This work was supported by Walloon Region (program First spin-off), FNRS (Fond National de la Recherche Scientifique), UIAP VII, ARC Programs of the French Community of Belgium, the Centre National de la Recherche Scientifique and the University Paul Sabatier. The support and sponsorship accorded by COST Actions D38 and TD1004 are kindly acknowledged. The authors thank Isabelle Mahieu for her help in cell cultures and the Center for Microscopy and Molecular Imaging (supported by the European Regional Development Fund and the Walloon Region).

REFERENCES

1. Tóth E, Helm L, Merbach AE. Relaxivity of gadolinium(III) complexes: theory and mechanism. In The Chemistry of Contrast Agents in Medical Magnetic Resonance Imaging, Merbach AS, Helm L, Tóth E (eds). John Wiley & Sons: Chichester, 2013; 25–82.
2. Sammes PG, Yahioglu G. Modern bioassays using metal chelates as luminescent probes. Nat Prod Rep 1996;13:1–28.
3. Jacquier A, Higgins CB, Saeed M. MR imaging in assessing cardiovascular interventions and myocardial injury. Contrast Media Mol Imag 2007;2:1–15.
4. Bunzli J-CG. Lanthanide luminescence for biomedical analyses and imaging. Chem Rev 2010;110:2729–2755.
5. Chan KW-Y, Wong W-T. Small molecular gadolinium(III) complexes as MRI contrast agents for diagnostic imaging. Coord Chem Rev 2007;251:2428–2451.
6. Brunet E, Juanes O, Rodriguez-Ubis J-C. Supramolecularly organized lanthanide complexes for efficient metal excitation and luminescence as sensors in organic and biological applications. Curr Chem Biol 2007;1:11–39.
7. Manning HC, Goebel T, Thompson RC, Price RR, Lee H, Bornhop DJ. Targeted molecular imaging agents for cellular-scale bimodal imaging. Bioconjug Chem 2004;15:1488–1495.
8. Laurent S, Vander Elst L, Wautier M, Galaup C, Muller RN, Picard C. In vitro characterization of the Gd complex of [2,6-pyridinediylbis (methylene nitrilo)] tetraacetic acid (PMN-tetraacetic acid) and of its Eu analogue, suitable bimodal contrast agents for MRI and optical imaging. Bioorg Med Chem Lett 2007;17:6230–6233.
9. Chellquist EM, Searle R. An LC method for measuring complex formation equilibria by competitive chelation. J Pharm Biomed Anal 1993;11(10):985–992.
10. Wedeking P, Kumar K, Tweedle MF. Dissociation of gadolinium chelates in mice: relationship to chemical characteristics. Magn Reson Imag 1992;10:641–648.
11. Bonnet CS, Buron F, Caillé F, Shade CM, Drahos B, Pellegatti L, Zhang J, Villette S, Helm L, Pichon C, Suzenet F, Petoud S, Toth E. Pyridine-based lanthanide complexes combining MRI and NIR luminescence activities. Chem Eur J 2012;18:1419–1431.
12. Martikkala E, Lehmusto M, Lilja M, Rozwandowicz-Jansen A, Lunden J, Tomohiro T, Hänninen P, Petäjä-Repo U, Härmä H. Cell-based β2-adrenergic receptor-ligand binding assay using synthesized europium-labeled ligands and time-resolved fluorescence. Anal Biochem 2009;392:103–109.
13. Gunanathan C, Pais A, Furman-Haran E, Seger D, Eyal E, Mukhopadhyay S, Ben-David Y, Leitus G, Cohen H, Vilan A, Degani H, Milstein D. Water-soluble contrast agents targeted at the estrogen receptor for molecular magnetic resonance imaging. Bioconjug Chem 2007;18:1361–1365.
14. Féau C, Klein E, Kerth P, Lebeau L. Synthesis of a coumarin-based europium complex for bioanalyte labeling. Bioorg Med Chem Lett 2007;17:1499–1503.
15. Havas F, Leygue N, Danel M, Mestre B, Galaup C, Picard C. 6,6′-Dimethyl-2,2′-bipyridine-4-ester a pivotal synthon for building tethered bipyridine ligands. Tetrahedron 2009;65:7673–7686.
16. Maindron N, Poupart S, Hamon M, Langlois J-B, Plé N, Jean L, Romieu A, Renard P-Y. Synthesis and luminescence properties of new red-shifted absorption lanthanide(III) chelates suitable for peptide and protein labelling. Org Biomol Chem 2011;9:2357–2370.
17. Takalo H, Mukkala V-M, Meriö L, Rodriguez-Ubis J-C, Sedano R, Juanes O, Brunet E. Development of luminescent terbium(III)

chelates for protein labelling: effect of triplet state energy level. Helv Chim Acta 1997;80:372–387.
18. Mukkala V-M, Sund C, Kwiatkowski M, Pasanen P, Högberg M, Kankare J, Takalo H. New heteroatomic complexing agents and luminescence of their europium(III) and terbium(III) chelates. Helv Chim Acta 1992;75:1621–1632.
19. Charier S, Ruel O, Baudin J-B, Alcor D, Allemand J-F, Meglio A, Jullien L, Valeur B. Photophysics of a series of efficient fluorescent pH probes for dual-emission-wavelength measurements in aqueous solutions. Chem Eur J 2006;12:1097–1113.
20. Autiéro H, Bazin H, Mathis G. Novel rare earth metal cryptates which are not very sensitive to the fluorescence quenching. PCT Int. Appl., WO 096877; Chem Abstr, 136:50664, 2001.
21. Feely WE, Beavers EM. Cyanation of amine oxide salts. A new synthesis of cyanopyridines. J Am Chem Soc 1959;81:4004–4007.
22. Liu P, Chen Y, Deng J, Tu Y. An efficient method for the preparation of benzylic bromides. Synthesis 2001;14:2078–2080.
23. Laumonier C, Segers J, Laurent S, Michel A, Coppée F, Belayew A, Vander Elst L, Muller RN. A New peptidic vector for molecular imaging of apoptosis, identified by phage display technology. J Biomol Screen 2006;11:537–545.
24. Solomon I. Relaxation processes in a system of two spins. Phys Rev 1955;99:559–565.
25. Bloembergen N. Proton relaxation times in paramagnetic solutions. J Chem Phys 1957;27:572–573.
26. Freed JH. Dynamic effects of pair correlation functions on spin relaxation by translational diffusion in liquids. II. Finite jumps and independent T1 processes. J Chem Phys 1978;68:4034–4037.
27. Vander Elst L, Raynal I, Port M, Tisnès P, Muller RN. In vitro relaxometric and luminescence characterization of P792 (Gadomelitol, Vistarem®), an efficient and rapid clearance blood pool MRI contrast agent. Eur J Inorg Chem 2005;6:1142–1148.
28. Laurent S, Vander Elst L, Muller RN. Comparative study of the physicochemical properties of six clinical low molecular weight gadolinium contrast agents. Contrast Media Mol Imag 2006;1:128–137.
29. Kang SI, Ranganathan RS, Emswiler JE, Kumar K, Gougoutas JZ, Malley MF, Tweedle MF. Synthesis, characterization, and crystal structure of the gadolinium(III) chelate of (1R,4R,7R)-α,α′,α″-trimethyl-1,4,7,10-tetraazacyclododecane-1,4,7-triacetic acid (DO3MA). Inorg Chem 1993;32:2912–2918.
30. Port M, Raynal I, Vander Elst L, Muller RN, Dioury F, Ferroud C, Guy A. Impact of rigidification on relaxometric properties of a tricyclic tetraazatriacetic gadolinium chelate. Contrast Med Mol Imag 2006;1:121–127.
31. Laurent S, Botteman F, Vander Elst L, Muller RN. Optimising the design of paramagnetic MRI contrast agents: influence of backbone substitution on the water exchange rate of Gd-DTPA derivatives. Magn Reson Mater Phys, Biol Med 2004;16:235–245.
32. Powell DH, Ni Dhubhghaill OM, Pubanz D, Helm L, Lebedev YS, Schlaepfer W, Merbach AE. Structural and dynamic parameters obtained from ^{17}O NMR, EPR, and NMRD studies of monomeric and dimeric Gd^{3+} complexes of interest in magnetic resonance imaging: an integrated and theoretically self-consistent approach. J Am Chem Soc 1996;118:9333–9346.
33. Livramento JB, Sour A, Borel A, Merbach AE, Toth E. A Starburst-shaped heterometallic compound incorporating six densely packed Gd^{3+} ions. Chem Eur J 2006;12:989–1003.
34. Zhang S, Jiang X, Sherry AD. Modulation of the lifetime of water bound to lanthanide metal ions in complexes with ligands derived from 1,4,7,10-tetraazacyclododecane tetraacetate (DOTA). Helv Chim Acta 2005;88:923–935.
35. Aime S, Botta M, Fasano M, Terreno E. Lanthanide(III) chelates for NMR biomedical applications. Chem Soc Rev 1998;27:19–29.
36. Laurent S, Henoumont C, Vander Elst L, Muller RN. Synthesis and physicochemical characterisation of Gd-DTPA derivatives as contrast agents for MRI. Eur J Inorg Chem 2012;12:1889–1915.
37. Laurent S, Vander Elst L, Henoumont C, Muller RN. How to measure the transmetallation of a gadolinium complex. Contrast Media Mol Imag 2010;5:305–308.
38. Jung K-H, Kim H-K, Lee GH, Kang D-S, Park J-A, Kim KM, Chang Y, Kim T-J. Gd complexes of macrocyclic diethylenetriaminepentaacetic acid (DTPA) biphenyl-2,20-bisamides as strong blood-pool magnetic resonance imaging contrast agents. J Med Chem 2011;54:5385–5394.
39. Silvério S, Torres S, Martins AF, Martins JA, André JP, Helm L, Prata MIM, Santos AC, Geraldes CFGC. Lanthanide chelates of (bis)-hydroxymethyl-substituted DTTA with potential application as contrast agents in magnetic resonance imaging. Dalton Trans 2009;24:4656–4670.
40. Laurent S, Parac-Vogt TN, Kimpe K, Thirifays C, Binnemans K, Muller RN, Vander Elst L. Bis(phenylethylamide) derivatives of Gd-DTPA as potential receptor-specific MRI contrast agents. Eur J Inorg Chem 2007;14:2061–2067.
41. Richardson FS. Terbium(III) and europium(III) ions as luminescent probes and stains for biomolecular systems. Chem Rev 1982;82:541–552.
42. Sabbatini N, Guardigli M, Lehn J-M. Luminescent lanthanide complexes as photochemical supramolecular devices. Coord Chem Rev 1993;123:201–228.
43. Armelao L, Quici S, Barigelletti F, Accorsi G, Bottaro G, Cavazzini M, Tondello E. Design of luminescent lanthanide complexes: from molecules to highly efficient photo-emitting materials. Coord Chem Rev 2010;254:487–505.
44. Supkowski RM, Horrocks WDW Jr. On the determination of the number of water molecules, q, coordinated to europium(III) ions in solution from luminescence decay lifetimes. Inorg Chim Acta 2002;340:44–48.
45. Beeby A, Clarkson IM, Dickins RS, Faulkner S, Parker D, Royle L, de Sousa AS, Williams JAG, Woods M. Non-radiative deactivation of the excited states of europium, terbium and ytterbium complexes by proximate energy-matched OH, NH and CH oscillators: an improved luminescence method for establishing solution hydration states. J Chem Soc, Perkin Trans 2 1999;3:493–503.
46. Alpha B, Balzani V, Lehn J-M, Perathoner S, Sabbatini N. Luminescence probes: the Eu^{3+} and Tb^{3+}cryptates of polypyridine macrobicyclic ligands. Angew Chem Int Ed Engl 1987;26:1266–1267.
47. Takalo H, Mukkala V-M, Mikola H, Liitti P, Hemmila I. Synthesis of europium(III) chelates suitable for labeling of bioactive molecules. Bioconjug Chem 1994;5:278–282.
48. Gutierrez F, Tedeschi C, Maron L, Daudey J-P, Poteau R, Azéma J, Tisnès P, Picard C. Quantum chemistry-based interpretations on the lowest triplet state of luminescent lanthanides complexes. Part 1. Relation between the triplet state energy of hydroxamate complexes and their luminescence properties. J Chem Soc Dalton Trans 2004;9:1334–1347.
49. De Bettencourt-Dias A. Small molecule luminescent lanthanide ion complexes – photophysical characterization and recent developments. Curr Org Chem 2007;11:1460–1480.
50. Werts MHV, Jukes RTF, Verhoeven JW. The emission spectrum and the radiative lifetime of Eu^{3+} in luminescent lanthanide complexes. Phys Chem Chem Phys 2002;4:1542–1548.
51. Nasso I. Complexes d'ions Ln(III) dérivés de ligands à motifs polyaminocarboxylique: synthèse, propriétés luminescentes (Eu^{III}, Tb^{III}) et relaxométriques (Gd^{III}). PhD Thesis, Paul Sabatier University, France, 2006.
52. Bruce JI, Dickins RS, Govenlock LJ, Gunnlaugsson T, Lopinski S, Lowe MP, Parker D, Peacock RD, Perry JJB, Aime S, Botta M. The selectivity of reversible oxy-anion binding in aqueous solution at a chiral europium and terbium center: signaling of carbonate chelation by changes in the form and circular polarization of luminescence emission. J Am Chem Soc 2000;122:9674–9684.
53. Dickins RS, Aime S, Batsanov AS, Beeby A, Botta M, Bruce JI, Howard JAK, Love CS, Parker D, Peacock RD, Puschmann H. Structural, luminescence, and NMR studies of the reversible binding of acetate, lactate, citrate, and selected amino acids to chiral diaqua ytterbium, gadolinium, and europium complexes. J Am Chem Soc 2002;124:12697–12705.
54. Moriggi L, Cannizzo C, Prestinari C, Berrière F, Helm L. Physicochemical properties of the high-field MRI-relevant $[Gd(DTTA\text{-}Me)(H_2O)_2]^-$ complex. Inorg Chem 2008;47:8357–8366.
55. Aime S, Geninatti Crich S, Gianolio E, Giovenzana GB, Tei L, Terreno E. High sensitivity lanthanide(III) based probes for MR-medical imaging. Coord Chem Rev 2006;250:1562–1579.
56. Vallet P. Relaxivity of nitroxide stable free radicals. Evaluation by field cycling method and optimisation, PhD Thesis, University of Mons-Hainaut, Belgium, 1992.
57. Laurent S, Vander Elst L, Copoix F, Muller RN. Stability of MRI paramagnetic contrast media a proton relaxometric protocol for transmetallation assessment. Invest Radiol 2001;36:115–122.
58. Nakamaru K. Synthesis, luminescence quantum yields and lifetimes of trischelated ruthenium(II) mixed-ligand complexes including 3,3′-2,2′bipyridyl. Bull Chem Soc Jpn 1982;55:2697–2705.
59. Meech SR, Phillips D. Photophysics of some common fluorescence standarts. J Photochem 1983;23:193–217.